

# The Far-Infrared Spectroscopy of the Troposphere (FIRST) Project

Martin G. Mlynczak, David G. Johnson, and Junilla I. Applin  
NASA Langley Research Center  
21 Langley Boulevard  
Hampton, VA 23681-2199

**Abstract.** The radiative balance of the Earth is influenced strongly by radiative cooling associated with emission of radiation by water vapor at far-infrared (far-IR) wavelengths greater than 15  $\mu\text{m}$  and extending out beyond 60  $\mu\text{m}$ . The distribution of water vapor and associated far-IR radiative forcings and feedbacks are well-recognized as major uncertainties in understanding and predicting future climate. Up to half of the outgoing longwave radiation (OLR) from the Earth occurs beyond 15.4  $\mu\text{m}$ . Cirrus clouds also modulate the outgoing longwave radiation in the far-IR. Despite this fundamental importance, far-IR emission (spectra or band-integrated) has rarely been directly measured from space, airborne, or ground-based platforms. Current and planned operational and research satellites typically observe the mid-infrared only to about 15.4  $\mu\text{m}$ . The Far-Infrared Spectroscopy of the Troposphere (FIRST) project is an investment by NASA through the Instrument Incubator Program (IIP) to develop a space-based capability to measure the spectrally resolved infrared spectrum to 100  $\mu\text{m}$ .

## I. INTRODUCTION

The radiation budget of the Earth system was the first quantitative measurement to be made from orbiting satellites, as proposed by Suomi [1]. Since that time, radiation budget measurements have consisted of the total (reflected solar plus emitted thermal infrared) radiation and the reflected solar radiation; these are spectrally integrated or broadband measurements with little spectral discrimination. The emitted longwave radiation is obtained by subtraction of the two classic energy flows. These measurements provide the integral constraints on the Earth's climate and energy budget. The response of and feedbacks within the Earth's climate system are determined by the terms of the integral, i.e., the absorption and emission spectra. Since the first observations by Suomi, radiation budget measurements have been refined significantly in terms of their spatial resolution, angular sampling capability, and radiometric calibration [2]. Temporal sampling is

improved by placing additional sensors in different orbit planes or, as planned in the near future, by placing radiation budget sensors in geostationary orbit [3]. Despite these continuous improvements, radiation sensors are still making the same basic measurements as 40 years ago with little additional spectral distinction. As pointed out by Wielicki *et al.* [2], sensing of the Earth's energy balance is an eight dimensional sampling problem. The improvements noted above in spatial, angular, and temporal sampling address seven of the eight dimensions. The remaining critical dimension, the spectral dependence of the radiation balance, and the far-IR in particular, have yet to be comprehensively observed from space. The Far-Infrared Spectroscopy of the Troposphere (FIRST) program represents NASA's investment in the technology required to measure the Earth's emission spectrum in order to achieve a significant advance in climate sensing.

## II. RELEVANCE OF THE FAR-IR TO THE GLOBAL ENERGY CYCLE, CLIMATE, AND WATER VAPOR PROFILING

### A. Clear-Sky Radiative Cooling

We define the far-IR to encompass wavelengths between 15 and 100  $\mu\text{m}$  because, as discussed below, this portion of the Earth's emission spectrum is not directly observed from space despite its fundamental importance. The radiative balance of the troposphere, and hence climate, is influenced strongly by radiative cooling associated with emission of infrared radiation by water vapor at far-IR wavelengths extending out beyond 60  $\mu\text{m}$  [4]. Water vapor absorption and emission are principally modulated by the pure rotation band, which includes both line and continuum absorption. Water vapor is the principal greenhouse gas, absorbing a significant fraction of the upwelling radiation [5] and providing much of the downwelling longwave flux that warms the Earth's surface (i.e., the greenhouse effect). The distribution of water vapor and associated radiative forcings and feedbacks (which occur in the far-IR) are well recognized as major uncertainties in understanding and predicting future climate [6-8].

The importance of the far-IR in the Earth's energy balance is readily assessed by computing the fraction of radiant energy emitted by the Earth-Atmosphere system at those wavelengths. Line-by-line radiative transfer calculations using the code of Kratz *et al.* [9] and discussed by Kratz [10] indicate that approximately 50%, 30%, 12% and 6% of the Earth's clear-sky thermally emitted power (outgoing long-wave radiation, OLR) occurs at wavelengths longer than 15, 20, 30, and 40  $\mu\text{m}$ , respectively. Approximately 60%, 40%, 18%, and 10% of the atmospheric thermally emitted power occurs at wavelengths longer than 15, 20, 30, and 40  $\mu\text{m}$ , respectively, depending on latitude and season. Measurements of the far-IR will contribute significantly to understanding how the Earth is responding to various natural and anthropogenic forcings, which is a fundamental goal of NASA's Earth Science Enterprise.

One of the basic roles water vapor plays in the climate system is in the radiative cooling of the troposphere [4] as dramatically illustrated in Figure 1 from Mertens *et al.* [11]. The figure shows the

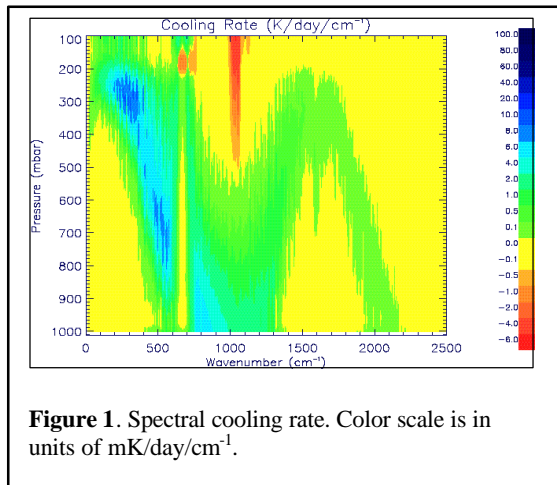


**Figure 1.** Spectral cooling rate. Color scale is in units of  $\text{mK}/\text{day}/\text{cm}^{-1}$ .

spectral cooling rate in the troposphere ( $\text{K}/\text{day}/\text{cm}^{-1}$ ) from 10 to 2500  $\text{cm}^{-1}$  (1000 to 4  $\mu\text{m}$ ) from the surface (1000 mb) to 100 mb (approximately 16 km altitude). The cooling rates are calculated with the LINEPAK line-by-line code [12] for clear sky using the Intercomparison of Radiation Codes in Climate Models (ICRCCM) midlatitude summer profiles [13]. The green-colored band between about 1300 and 2100  $\text{cm}^{-1}$  represents the cooling by the vibration-rotation bands of water vapor in the mid-infrared. Strong radiative cooling in the far-IR, due to water vapor rotational and continuum emission, occurs between 100 and 500  $\text{cm}^{-1}$  (indicated by the blue colors). This figure clearly illustrates that far-infrared emission by water vapor is responsible for cooling

the atmosphere from the surface to around 200 mb. The bulk of the free troposphere cools radiatively in the far-IR portion of the spectrum.

### B. Clear-Sky Greenhouse Effect

Water vapor is also a principal factor the Earth's greenhouse effect. Shown in Figure 2 is the difference between the (Planck blackbody) emission from the Earth's surface and the energy emitted to space. The curve indicates the energy trapped by the atmosphere and is called the greenhouse parameter. We can see from this curve that the greenhouse trapping is caused by the  $\nu_2$  band of water vapor above about 1400  $\text{cm}^{-1}$ , ozone at 1060  $\text{cm}^{-1}$ ,  $\text{CO}_2$  between 600 and 700  $\text{cm}^{-1}$ , and the pure rotation band of water vapor between 0 and about 800  $\text{cm}^{-1}$ . This latter water band is extremely intense, especially at band center around 200-300  $\text{cm}^{-1}$ , and so emits to space from the upper troposphere, precisely where the temperature is low enough to move the peak of the Planck function to this same wavenumber range. This is also the physical cause of the cooling illustrated in Figure 1. Spectral measurements, with complete spectral coverage of the infrared to 100  $\mu\text{m}$ , will enable a comprehensive assessment of the Earth's greenhouse effect including forcings and feedbacks.

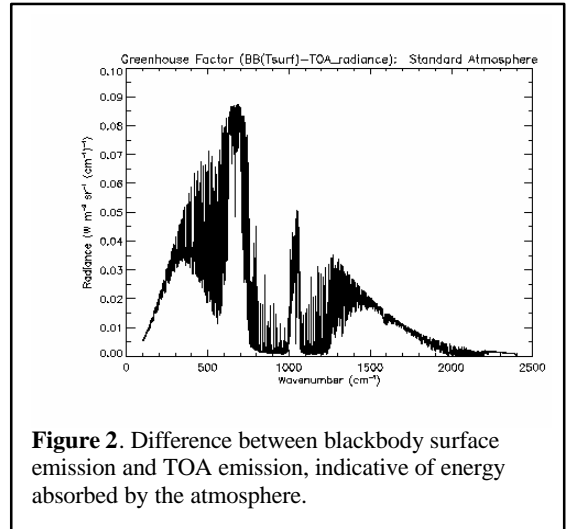


**Figure 2.** Difference between blackbody surface emission and TOA emission, indicative of energy absorbed by the atmosphere.

### C. The Influence of Cirrus Clouds

The above calculations are for clear-sky conditions. We also note that the outgoing far-infrared radiation will be modulated by cirrus clouds. The prevalence and persistence of cirrus cloud systems, especially in the tropical upper atmosphere, implies that cirrus clouds play an important role in

climate [14]. Cirrus clouds have always represented a formidable modeling challenge owing to the extreme conditions under which the ice crystals form and to their complex radiative interactions [15]. Bulk radiative studies of cirrus clouds show that cirrus clouds may radiatively heat or cool the upper atmosphere at infrared wavelengths depending upon the height, thickness and microphysical size of the clouds [16-18]. Cirrus clouds have also been implicated as important components of feedback loops to climate forcings [19-21]. The effects of cirrus in attenuating the far-IR OLR to 25  $\mu\text{m}$  have been shown from the space measurements made by the Russian *Meteor* spacecraft [22] and in the calculations of Stackhouse and Stephens [18]. Far-IR measurements also offer the opportunity to determine cirrus cloud properties [23].

#### D. Improvement in Water Vapor Profiling

Spectral measurements of the far-IR may also offer the potential for increased accuracy in water vapor profiles retrieved from emission measurements. Water vapor, particularly in the upper troposphere, is the dominant greenhouse gas and largest known feedback mechanism for amplifying global warming, contributing more than two-thirds of the total feedback by water vapor [24]. The processes that govern its concentration have been the subject of long-standing debate [6] and still remain uncertain [25] partially reflecting the lack of adequate observations of water vapor [26]. Model predictions of global temperature increases resulting from continued buildup of greenhouse gases depend on the treatment of water vapor [27] and on the absence of a negative feedback by water vapor in the upper troposphere, the occurrence of which is not yet certain [28,29]. Improved measurements of water vapor and far-IR emissions will help address this issue.

Infrared water vapor vertical profiling from space for the past 30 years in both operational and research sensors has been limited to measurements of thermal emission in the  $\nu_2$  band centered at 6.3  $\mu\text{m}$ . However, some of the very first space-based measurements attempted for the purpose of water vapor profiling were in the far-IR with the SIRS-B instrument [30]. Due to strong emission from the upper troposphere in the far-IR, there is a very high probability that the combination of (simultaneous) far-IR and conventional mid-IR radiance measurements will result in more accurate water profiles with higher vertical resolution than is available from measurements of the 6.3  $\mu\text{m}$  band

alone, especially in the upper troposphere. The potential for far-IR sounding of tropospheric water vapor is discussed by Mertens *et al.* [31].

### III. PRIOR AND EXISTING FAR-IR MEASUREMENTS

Despite the recognized importance of the far-IR, there are no currently identified NASA, NOAA, NPOESS or international missions or selected mission candidates with capability to directly (spectrally) sense the Earth and atmosphere far-IR emission. The far-IR spectrum beyond 15  $\mu\text{m}$  was last measured from space on two Russian *Meteor* spacecraft launched 26 years ago [32] and over 30 years ago by the IRIS instruments on the NASA Nimbus III and IV spacecraft [33, 34], and then only to 25  $\mu\text{m}$  ( $400\text{ cm}^{-1}$ ) with relatively coarse spectral (several  $\text{cm}^{-1}$ ) and spatial resolution. The primary difficulty in measuring the far-IR with high spatial resolution (and high precision) has been the cryogenic cooling demands of prior long-wave detectors and optical systems. Advances in passively cooled pyroelectric detectors and microbolometers [35-38] offer the potential for far-IR measurements to be made with passively cooled detector systems thus obviating the need for active or passive cryogenic cooling and thereby eliminating the attendant mass, power, size, and lifetime penalties associated with spaceflight of such systems.

At present and in the foreseeable future there are no planned space-based spectral measurements extending out beyond about 15  $\mu\text{m}$ . Spectral instruments flying on NASA's Earth Observing System (AIRS and MODIS) do not have channels that measure the far-IR and are not sensitive beyond 15.4  $\mu\text{m}$ . The IASI instrument on the European METOP satellite (launch ~ 2003) is another spectral instrument sensitive only to 15.5  $\mu\text{m}$ . The Tropospheric Airborne Fourier Transform Spectrometer (TAFTS, an aircraft instrument), developed at Imperial College of Science, Technology, and Medicine (ICSTM) in London, UK flew successfully for the first time in September, 1999. TAFTS is sensitive from 10  $\mu\text{m}$  to 120  $\mu\text{m}$  with a spectral resolution of 0.1  $\text{cm}^{-1}$ . In addition, a Radiation Explorer in the Far-Infrared (REFIR) satellite experiment has been through Phase A development and is described further by Palchetti *et al.* [39]. The primary instrument on the REFIR mission is a Fourier Transform Spectrometer nominally covering the spectral range from 10 to 100  $\mu\text{m}$  at a resolution of 0.5  $\text{cm}^{-1}$ . There are as yet no direct far-IR measurements selected for spaceflight.

Although there have been few spectrally-resolved measurements of the far-IR emission, there have been broadband measurements of the OLR which were sensitive to far-IR emission. Specifically, the Earth Radiation Budget Experiment (ERBE) scanner instrument [40] measured reflected solar radiation and emitted terrestrial radiation in 3 channels: a shortwave channel, 0.2 to 5.0  $\mu\text{m}$ ; a longwave channel, 5 to 50  $\mu\text{m}$ , and a total channel, 0.2 to 200  $\mu\text{m}$ . The ERBE scanner longwave and total channels are sensitive to far-IR emission. Presently, the Clouds and the Earth's Radiant Energy System (CERES) [2] instrument is operating on the EOS Terra satellite. It will also be operating on the EOS Aqua satellite. CERES has three spectral channels: a total channel, 0.2 to 100  $\mu\text{m}$ , a shortwave channel, 0.2 to 5  $\mu\text{m}$ , and a window channel, 8-12  $\mu\text{m}$ . The longwave 5  $\mu\text{m}$  to 100  $\mu\text{m}$  is obtained by subtraction. In addition, the Geostationary Earth Radiation Budget (GERB) Experiment [3] senses radiation in the 0.32 to 4.0  $\mu\text{m}$  and in the 0.32 to 50  $\mu\text{m}$  intervals. The range 4 to 50  $\mu\text{m}$  is obtained by subtraction. The first GERB is to be launched in 2002, and additional instruments will be launched approximately every 3 years on the METEOSAT platform. CERES and GERB are the only two instruments in (or soon to be in) orbit that are sensitive to far-IR emission.

#### IV. SCIENCE IMPACT OF FAR-IR MEASUREMENTS

In short, far-IR measurements are crucial to understanding the Earth's climate. Space-based measurements of the far-IR emission would enable the scientific community:

- To achieve a more comprehensive understanding of the Earth's energy cycle by directly observing the radiative cooling effects of tropospheric water vapor in the far-IR,
- To obtain a more accurate understanding of the radiative impact of cirrus clouds on climate by directly observing their radiative and microphysical properties at far-IR wavelengths, and
- To realize significantly improved knowledge of water vapor in the upper troposphere.

Each of these will radically improve our ability to model, and hence predict the future of the Earth system. Nothing can substitute for direct observations of key radiative and thermodynamic processes.

#### V. INSTRUMENT AND SYSTEM REQUIREMENTS FOR FAR-IR SPACE-BASED MEASUREMENTS

To achieve the above science from a space instrument, we would require the following measurement capability (as discussed further by Johnson [41]):

- Spectral coverage: 4 - 100  $\mu\text{m}$  (essentially the entire thermal infrared).
- Spectral resolution: 0.6  $\text{cm}^{-1}$
- Nadir viewing IFOV, satellite instrument: 10 km spatial footprint
- Broad cross-track observational capability to provide global coverage on a daily basis
- Passive cooling of optical and detector systems to  $\sim 180$  Kelvin
- NE $\Delta$ T: 0.2 K 10 to 100  $\mu\text{m}$  (goal); 0.2 K 10 to 60  $\mu\text{m}$ , 0.5 K 60 to 100  $\mu\text{m}$  (requirement)

The spectral coverage is driven by the need to measure the unobserved far-IR together with the CO<sub>2</sub> 15  $\mu\text{m}$  band for temperature retrievals and validation against existing mid-IR sensors. The spectral resolution of 0.6  $\text{cm}^{-1}$  is driven primarily by the requirement to simultaneously retrieve temperature profiles. The IFOV is driven by the need to be able to isolate clear and cloudy fields of view. The daily global coverage capability, which impacts primarily the detector focal plane array, is to ensure global observations of water vapor and that as much as possible of the natural spatial variability in the radiation and cloud fields is observed. Passive cooling to temperatures achievable in the space environment ( $\sim 180$  K) for the optical system and detectors is essential to avoid the mass, power, volume, and lifetime penalties associated with mechanical cryogenic systems or dewars of liquid helium. The temperature sensitivity of 0.2 K is required for temperature profiling and to detect the climate change fingerprint. Our vision is to develop space-based instrumentation to cover the entire spectral range from 4  $\mu\text{m}$  to 100  $\mu\text{m}$  in order to fully measure the Earth's thermal infrared at high spatial and spectral resolution for both Earth radiation budget sensing and atmospheric temperature and moisture profiling.

#### VI. FAR-INFRARED SPECTROSCOPY OF THE TROPOSPHERE (FIRST) TECHNOLOGY DEVELOPMENT

The FIRST project was selected by NASA in late 2002 in response to a proposal submitted to the NASA Research Announcement NRA-01-OES-01.

FIRST will develop and demonstrate a Michelson interferometer capable of sensing the spectral region between 10 and 100  $\mu\text{m}$  (1000 to 100  $\text{cm}^{-1}$ ) at 0.6  $\text{cm}^{-1}$  resolution (unapodized). It will advance technology in three specific areas: the interferometer itself; broad bandpass beamsplitters; and far-infrared sensitive detectors.

We will meet our goal of daily global coverage with a 10 km footprint by designing a single-band spectrometer with an imaging detector that provides a spectrum with the required sensitivity in less than 1.7 s. Performance requirements are derived by assuming an orbital sampling configuration similar to that being developed for the NPOESS Crosstrack Infrared Sounder (CrIS). CrIS collects an array of atmospheric radiance samples in a  $\pm 48^\circ$  horizon-to-horizon sweep as the satellite moves around the globe in a sun-synchronous low earth orbit. To achieve a spatial resolution of 10 km the spectrometer must produce spectra of roughly 5,000,000 fields per day. For a single detector (non-imaging) instrument this corresponds to 17 ms per spectrum (including the time to acquire the next field-of-view (FOV)). This far exceeds the capability of existing detector technology. For example, to record a 2-sided interferogram in 17 ms that produces a spectrum covering the band from 10 to 100  $\mu\text{m}$  with a resolution of 0.6  $\text{cm}^{-1}$ , the detector requires an electronic bandwidth of 9 to 90 kHz. By utilizing multiple detectors in the FOV, we can increase the available measurement time per FOV by a factor equal to the number of pixels in the focal plane. Using a modest 10 by 10 array, in 15 steps across the same  $\pm 48^\circ$  sweep, we increase the time per FOV sample to 1.7 s and reduce the bandwidth requirement to 90-900 Hz, well within the range of current pyroelectric detectors.

#### A. FIRST Instrument Description

In this section we present our design approach for a spectrometer capable of meeting the satellite measurement requirements. An FTS is the best choice for the spectrometer, because of our need to provide spectra covering a factor of 10 in wavelength, the fact that we will be detector noise (rather than photon noise) limited due to our use of passively cooled detectors, and the large sample angles required to acquire the 100 x 100 km FOV (using a 10 x 10 detector array). Our breakthrough design has been made possible as a result of recent advances in bilayer beamsplitters, pyroelectric detectors, and high-throughput imaging FTS designs.

#### B. Design Requirements

Despite advances in beamsplitter efficiency and detector sensitivity, achieving the required sensitivity and FOV with a passively cooled spectrometer requires a state-of-the-art FTS with very high throughput. Detecting the climate change fingerprint requires a spectral noise equivalent change in temperature (NEdT) of 0.2 K. This requires a signal to noise ratio (SNR) of 350, 545, and 656 at 500  $\text{cm}^{-1}$  (20  $\mu\text{m}$ ), 278  $\text{cm}^{-1}$  (36  $\mu\text{m}$ ), and 200  $\text{cm}^{-1}$  (50  $\mu\text{m}$ ), respectively.

The maximum throughput for a given instrument volume is achieved with a 2-port Michelson design. By using plane mirrors rather than retroreflectors we minimize the optical path inside the spectrometer, reducing the effect of beam divergence and further increasing the throughput. Note that the use of plane mirrors rules out Martin-Puplett and conventional 4-port designs. We achieve the maximum possible flux concentration on each detector by using Winston cones [42] to achieve an  $f/0.5$  beam. The  $f$ -number is given by  $1/(2\sin\theta)$ , where  $\theta$  is half the divergence angle, so that an  $f/0.5$  beam accepts light from  $\pm 90^\circ$  and thus fills one hemisphere of the detector FOV. For a scene temperature of 230 K, assuming that the spectrometer throughput is sufficient to fill the beams of all the Winston cones in the focal plane, the band-averaged SNR (10-100  $\mu\text{m}$ ) of such a system is given by  $(4.6 \times 10^{-6} \text{ W cm}^{-2} \text{ Hz}^{-0.5}) \times (D^* A_d^{0.5})$ , where  $D^*$  and  $A_d$  are the detector detectivity and area, respectively, and we have assumed that  $D^*$  is independent of  $A_d$ . For this calculation we have assumed that of the 1.7 s available for each FOV we use 1.4 s to record the spectrum, and that the overall system efficiency is 0.21 (note that the efficiency for an ideal 2-port Michelson is 0.25).

The best presently available pyroelectric detectors have a maximum detectivity of  $10^9 \text{ cm Hz}^{0.5} \text{ W}^{-1}$  at 1 kHz. To achieve a band-averaged SNR of 500 (to meet the SNR requirement of 545 at 36  $\mu\text{m}$ ) we need a detector area of 0.012  $\text{cm}^2$  behind the Winston cone. Filling the beams of a 10x10 array of Winston cones that are matched to this detector requires an instrument throughput of 3.71  $\text{cm}^2 \text{ sr}$ , which would be difficult to achieve. For a detector that achieves the thermal noise limit of  $1.8 \times 10^{10} \text{ cm Hz}^{0.5} \text{ W}^{-1}$  at 300 K, the required detector area is  $3.5 \times 10^{-5} \text{ cm}^2$  (66  $\mu\text{m}$  pixels) and the spectrometer throughput is reduced to 0.011  $\text{cm}^2 \text{ sr}$ , which is comfortably within the range of existing designs. For comparison, the detectivity of a photon noise limited detector would be  $\sim 10^{11} \text{ cm Hz}^{0.5} \text{ W}^{-1}$  for a 230 K scene temperature.

The ability to fabricate Winston cones with the desired accuracy and the need for sensitivity at a wavelength of 100  $\mu\text{m}$  place a lower limit on the size of the detector. For example, the smallest exit aperture presently available from Infrared Labs is 254  $\mu\text{m}$ , which is sufficiently large that diffraction effects do not degrade the performance at a wavelength of 100  $\mu\text{m}$ . Filling the beams of a 10x10 array of such cones requires a spectrometer throughput of 0.3  $\text{cm}^2$  sr. One may question the value of using Winston cones if doing so requires such large pixels. Illuminating a pixel array directly using an f/2.5 beam (which is about as fast as can be achieved with off-axis optics) instead of using Winston cones reduces the predicted SNR by a factor of 13, showing that there is a substantial advantage to be gained by using the cones.

The FIRST interferometer is being designed and built by the Space Dynamics Laboratory (SDL) at Utah State University (USU). SDL has a multi-decade heritage of providing FTS-based sensors for low-earth and geostationary orbit, aircraft, and balloon platforms. The design exploits Langley (LaRC) and SDL experience to integrate large format detector arrays into a proven FTS design to provide the high spatial resolution and coverage rates required by this revolutionary sensor. The FIRST spectrometer is designed to meet the critical performance requirements of a satellite sensor. FIRST will be demonstrated on a balloon platform to minimize impacts of acoustic and mechanical noise and vibration. The interferometer, aft optics, and the detector array assembly will be cryogenically cooled to 180 K during the balloon flight demonstration to simulate the temperatures achievable by passive cooling (i.e., without cryogenics) in a space environment. The FIRST FTS system will be mounted in a vacuum Dewar with a polypropylene window to minimize cooling requirements and acoustic coupling to the thin-film beamsplitter.

### C. FTS Subsystem

The interferometer will use the 45° beamsplitter design that has flown successfully on several missions (EXCEDE I, II, SPIRIT, CIRRIS-1A and BAMB) and is being used on the Geostationary Imaging Fourier Transform Spectrometer (GIFTS) sensor being developed by LaRC and SDL. The design uses a precision machined, solid block flex-pivot porch swing suspended carriage. The SDL design provides a full +/- 0.8 cm drive range with mirror alignment accuracy better than +/- 2  $\mu\text{rad}$  and repeatability better than 0.2  $\mu\text{rad}$ . Metrology is

provided by a laser based quadrature sampling control system that counts fringes through the carriage turnaround. While the space flight system would use a stabilized diode laser, a HeNe laser will be used in FIRST. Frequency stability better than 1 part in  $5 \times 10^6$ , is required. The laser will be mounted in the electronics (warm) section of FIRST, with the output of the laser coupled to the interferometer metrology system via fiber optics. Errors that arise from scan velocity variations are minimized by a precision scan drive and optical path difference (OPD) velocity servo system to control the scan speed to better than +/-1 percent. The FIRST cube design will leverage the design work done for GIFTS, with the aperture size and beamsplitter mount modified for FIRST. The nominal beam diameter and divergence angle are 7.0 cm and 0.1 rad, respectively, giving a spectrometer throughput of 0.475  $\text{cm}^2$  sr. The design will be optimized for accurate radiometric imaging.

### D. Aft Optics and Detector Array Mounting

FIRST uses the compact all-reflective aft optical system developed for GIFTS, scaled to FIRST aperture size and f/#. A diagram of this system is shown in Figure 3. The optics will be gold-coated aluminum for low cost and high reflectivity in the far infrared. The optic system is f/4.4 and allows the interferometer to handle a 6° beam divergence. The FIRST optical aperture (on the interferometer mirrors) is sized to match the FPA assembly (the 10 x

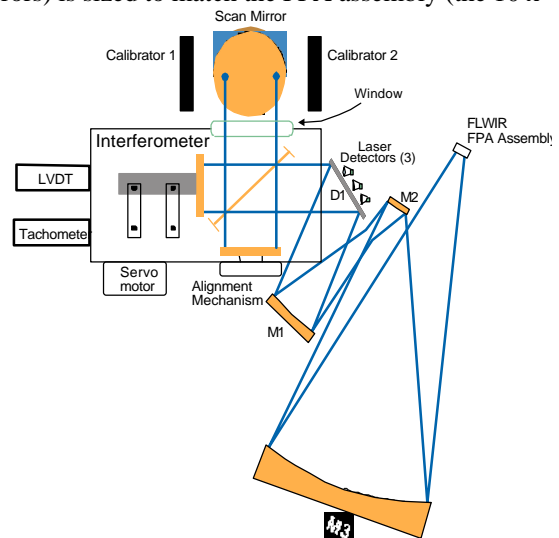


Figure 3. FIRST FTS layout.

10 array of Winston cones which couple the detectors to the optical beam.) To reduce cost, the 10x10 array

will be only partially filled. Standard cones from Infrared Laboratories, Inc. (Model F4.40#00, f/4.40) have been used in this design. The cones are mated to 254  $\mu\text{m}$  diameter sensor elements, spaced in an array on 2.2 mm centers.

### *E. The Beamsplitters*

The recent development of wide-band beamsplitters that work well in the far infrared now make it possible to use a single FTS to cover the 10–100  $\mu\text{m}$  band. These include lithographic polarizing (for Martin-Puplett interferometers) and bilayer beamsplitters (for conventional Michelson interferometers), both of which have demonstrated nearly ideal performance over the required band. The FIRST beamsplitters will be developed at the Smithsonian Astrophysical Observatory (SAO) as part of its ongoing programs of FIRS-2 instrument development and high-resolution stratospheric measurements [43, 44]. These beamsplitters are constructed of 2 thin dielectric layers, with thickness chosen to give nearly equal 50% transmission and reflection coefficients over a very wide wavelength range in the far and near infrared [45]. The spectral range covered by these beamsplitters includes the entire range required by the FIRST design.

A preliminary version of the bilayer beamsplitter has been deployed in the FIRS-2 instrument to obtain atmospheric observations. This beamsplitter (Ge on Mylar) gave us the expected spectral response when flown on a balloon at long wavelengths (120 to 14  $\mu\text{m}$ ), however the performance between 14 and 6  $\mu\text{m}$  fell short of optimum due to unwanted absorption features in the Mylar between 14 and 6  $\mu\text{m}$ . Optically, polypropylene is a significantly more transparent material in the far infrared than Mylar, with only a few weak and narrow absorptions near 11  $\mu\text{m}$ , so it is an ideal replacement material from this point of view. However, the bulk thermal and mechanical properties are not as ideal for evaporative deposition as that of Mylar as it melts easily under evaporation chamber heat loads. A method has been devised that allows us to cope with the heat load, and which allows us to deposit 1  $\mu\text{m}$  thick layers of Ge onto thin polypropylene sheets with optical quality surfaces. We have access to an evaporator with all the necessary features for this process and have already made several very promising test versions of this beamsplitter design. We will continue to manufacture and test these beamsplitters in order to produce one that is ideal for FIRST with nearly unit efficiency between 120 and 9  $\mu\text{m}$ .

### *F. The Detectors*

FIRST takes advantage of recent advances in pyroelectric detector performance to provide a passively cooled far-infrared FTS with the required sensitivity. Previously, the detectors in a continuous-scan FTS operating at wavelengths beyond the HgCdTe cutoff wavelength (roughly 15  $\mu\text{m}$ ) were limited to liquid-Helium cooled photoconductors. While high-Tc superconducting bolometers have good sensitivity at liquid nitrogen temperatures, their useful electrical bandwidth is too narrow to use in the broadband FTS we propose. One portion of the FIRST effort will further improve a state-of-the-art pyroelectric detector design to reach the thermal noise limit at ambient temperature ( $\sim 180$  K in a passively cooled space environment).

Detector size, speed and long wavelength detection impose conflicting requirements on the detector. High speed and background-limited detectivity require the detector to be small, while the absorbing element needs to be comparable in size to the longest wavelength of interest. Therefore, the FIRST detector design will incorporate a microantenna for maximum absorption from 10–100  $\mu\text{m}$  in conjunction with a relatively small pyroelectric thermal sensor for fast response time. Microantennas have been used previously in superconducting microbolometers and uncooled thermal detectors for improved sensitivity in the far infrared [46]. A log-spiral design as shown in Figure 4 will be used to provide uniform response over the full band. In this design, the length of the antenna arm determines the long wavelength limit while the radius of the antenna feed determines the short wavelength limit. A YBaCuO thermometer will be impedance-matched to the antenna and suspended by micromachining techniques to maximize the responsivity. The small thermometer size provides low thermal mass, giving uniform electrical response for optical modulations ranging from 114–1140 Hz. A reflector geometry adapted from the double-mirror structure [47] developed for NASA Langley's CERES program will be used to efficiently couple the detector to the Winston cone and provide uniform optical response. By incorporating these features into the detector design we will increase the detectivity of  $\sim 10^9$   $\text{cm Hz}^{0.5}/\text{W}$  demonstrated previously [38] to  $\sim 10^{10}$   $\text{cm Hz}^{0.5}/\text{W}$ .

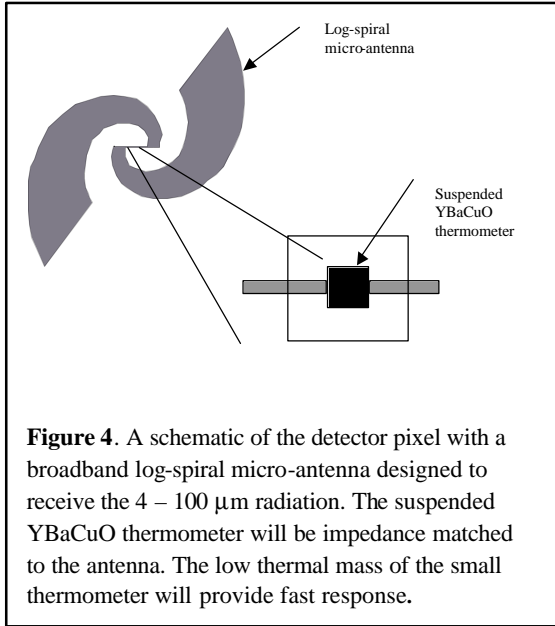


**Figure 4.** A schematic of the detector pixel with a broadband log-spiral micro-antenna designed to receive the 4 – 100  $\mu\text{m}$  radiation. The suspended YBaCuO thermometer will be impedance matched to the antenna. The low thermal mass of the small thermometer will provide fast response.

Responsivity, specific detectivity, and noise measurements will be performed up to 20- $\mu\text{m}$  wavelength laboratory facilities at SMU. Responsivity of individual prototype detectors beyond 20  $\mu\text{m}$  will be verified behind the selected Winston cone as part of the characterization process. We will also measure the relative responsivity over the full 10-100  $\mu\text{m}$  band as part of FIRST calibration as described in the next section. Thermal conductivity will be measured using a resistive heating method. Reflectivity and absorptivity of the structures will be analyzed. Other figures of merit such as pyroelectric coefficient and complex dielectric constant of the IR sensitive film will be characterized. Measurements will be performed over the temperature range of 100 to 300 K.

## VII. CALIBRATION

FIRST calibration will consist of two parts: preflight characterization and calibration, and field calibration. FIRST will be built and tested in a modular fashion, allowing subsystem performance to be verified before the sensor is fully integrated. Test and calibration procedures and initial performance model predictions will be validated using the extensive calibration procedures available from this team and the hardware from previous infrared sensor projects (DIRBE, SPIRIT III, SABER, GIFTS). Imaging FTS calibration techniques required for FIRST have been demonstrated using the SDL Imaging Interferometer Demonstrator.

### A. Preflight Characterization and Calibration.

The system will be thoroughly characterized and calibrated before the flight demonstration using the SDL Multi-function Infrared Calibration (MIC) system. End-to-end radiometric accuracy will be verified during instrument ground calibration using a highly accurate, NIST-traceable, large aperture blackbody over a range of cryogenic to ambient temperatures. The spectral shapes will be compared to the spectral shapes collected from SDL's NIST-verified smaller aperture blackbody source to validate the performance of the SDL extended sources at the longest wavelengths. As part of the IIP, a detailed calibration plan will be developed by SDL and FIRST partner G and A Technical Software (GATS), drawing on our experience in calibrating several NASA IR sensors. The imaging interferometer aspects required for FIRST will be verified on the SDL GIFTS demonstrator.

### B. Field calibration sources.

The FOV scanning system for FIRST will include two on-board blackbody calibration sources (at  $\sim 225$  K and 275K) that, along with a space look, provide high accuracy radiometric calibration. These sources are viewed twice per sweep, once in each interferometer scan direction. Several scans are point by point co-added to reduce spectral noise in the calibration. The difference between the two internal blackbody views provides the sensor slope term in the calibration equation, while the space look corrects for radiant emission from the instrument by establishing the offset term. The design follows the proven SDL blackbody extended source design, but is scaled to FIRST beam size (7 cm diameter). The baseline surface is Chemglaze Z306, with microspheres [48]. Source temperature is set by thermal strap tailoring between cold and warm regions, to achieve the desired temperature range with an array of sensors utilized for accurate absolute temperature measurement.

### C. Spectral Calibration

The FTS system used in FIRST has a well-understood instrument line shape (ILS) that depends mainly on well-characterized instrument parameters, e.g. the wavelength of the laser used for the detector trigger and the geometry of the focal plane relative to the interferometer axis. Moreover, precise measurements of ILS using a gas cell source will be obtained for each detector during the ground

characterization. The ILS can be represented as an ideal interferometer ILS and a sinc(x) function convolved with a simple function determined by the location in the array. The main effect is a highly predictable shift in spectral position. Techniques for correcting the off-axis position of each of the non-centered detectors have been developed under the GIFTS program. The frequency shifts and spectral line shape effects will be verified during characterization and accurately removed in ground data processing so that the FIRST data stream will be provided on a single spectral sampling grid with a normalized instrument line shape.

#### ACKNOWLEDGEMENT

The authors acknowledge the support of the Earth Science Technology Office of NASA and the Langley Research Center's Atmospheric Sciences and Systems Engineering Competencies for supporting the development of FIRST.

#### REFERENCES

1. V. E. Suomi, The radiation budget of the Earth from a satellite, NSF USNC IGY Project 30.11," Univ. of Wisconsin, **22** pp., 1957.
2. B. A. Wielicki, B. R. Barkstrom, E. F. Harrison, R. B. Lee III, G. L. Smith, and J. E. Cooper, Clouds and the Earth's radiant energy system (CERES): An Earth Observing System experiment, *Bull. Amer. Met. Soc.*, **77**, pp. 853-868, 1996.
3. J. E. Harries and D. Crommelynck, The Geostationary Earth Radiation Budget Experiment on MSG-1 and its potential applications, *Adv. Space Res.*, **24**, pp. 915-919, 1999.
4. S. A. Clough, J. Iacono, and J. L. Moncet, Line-by-line calculations of atmospheric fluxes and cooling rates: Application to water vapor, *J. Geophys. Res.*, **97**, pp. 15,761-15,785, 1992.
5. J. E. Harries, The greenhouse Earth: A view from space, *QJRMS*, **122**, pp. 799-818, 1996.
6. R. S. Lindzen, Some coolness concerning global warming, *Bull. Amer. Meteor. Soc.*, **71**, pp. 288-299, 1990.
7. M. T. Chahine, The hydrological cycle and its influence on climate, *Nature*, **359**, pp. 373-380, 1992.
8. J. E. Harries, Atmospheric radiation and atmospheric humidity, *QJRMS*, **123**, pp. 2173-2186, 1997.
9. D. P. Kratz, M.-D. Chou, M. M.-H. Yan, and C.-H. Ho, Minor trace gas radiative forcing calculations using the k distribution method with one parameter scaling, *J. Geophys. Res.*, **103**, pp. 31,647-31,656, 1998.
10. D. P. Kratz, High resolution modeling of the far-infrared, in *Optical Spectroscopic Techniques, Remote Sensing, and Instrumentation for Atmospheric and Space Research IV*, Allen M. Larar and Martin G. Mlynczak, Editors, Proceedings of SPIE, Vol. 4485, 171-180, 2002.
11. C. J. Mertens, M. G. Mlynczak, R. R. Garcia, and R. W. Portmann, A detailed evaluation of the stratospheric heat budget 1 Radiation transfer, *J. Geophys. Res.*, **104**, pp. 6021-6038, 1999.
12. L. L. Gordley, B. T. Marshall, and D. A. Chu, LINEPAK: Algorithms for modeling spectral transmittance and radiance, *J. Quant. Spectrosc. Radiat. Transfer*, **52**, pp. 563-580, 1994.
13. R. G. Ellingson, J. Ellis, and S. Fels, The intercomparison of radiation codes used in climate models: Long wave results, *J. Geophys. Res.*, **96**, pp. 8929-8953, 1991.
14. K.-N. Liou, Influence of cirrus clouds on weather and climate processes: a global perspective, *Mon. Wea. Rev.*, **114**, pp. 1167-1199, 1986.
15. V. Ramaswamy, and A. Detwiler, Interdependence of radiation and microphysics in cirrus clouds, *J. Atmos. Sci.*, **43**, pp. 2289-2301, 1986.
16. S. K. Cox, Cirrus clouds and the climate, *J. Atmos. Sci.*, **28**, pp.1513-1515, 1973.
17. G. L. Stephens, S.-C. Tsay, P.W. Stackhouse, and P.J. Flatau, The relevance of the microphysical and radiative properties of cirrus clouds to climate and climatic feedback, *J. Atmos. Sci.*, **47**, pp. 1742-1753, 1990.
18. P. W. Stackhouse, Jr., and G.L. Stephens, A theoretical and observational study of the radiative properties of cirrus clouds: results from FIRE 1986, *J. Atmos. Sci.*, **48**, pp. 2044- 2059, 1991.
19. D. A. Randall, Harchvardhan, D. A. Dazlich, and T.G. Corsetti, 1989: Interactions among radiation, convection and large-scale dynamics in a general circulation model, *J. Atmos. Sci.*, **46**, pp. 1943-1970.
20. A. K. Betts, Greenhouse warming and the tropical water budget, *Bull. Amer. Meteor. Soc.*, **71**, pp. 1464-1465, 1990.
21. A. D. Del Genio, M.-S., Yao, W. Kovari and K.K.-W. Lo, A prognostic cloud water parameterization for global climate models, *J. Climate*, **9**, 270-304, 1996.
22. D. Spankuch, and W. Dohler, Radiative properties of cirrus clouds in the middle IR derived from Fourier spectrometer measurements from space, *Z. Meteorol.*, **35**, pp. 314-324, 1985.
23. M. D. Vanek, I. G. Nolt, N. D. Tappan, P. A. R. Ade, F. C. Gannaway, C. Lee, P. A. Hamilton, K. F. Evans, J. E. Davis, and S. Predko, Far infrared sensor for cirrus (FIRSC): An aircraft based FTS to measure cloud radiance, *Appl. Opt.*, **40**, 2169-2176, 2001.
24. I. M. Held, and B.J. Soden, Water vapor feedback and global warming, *Ann. Rev. of Energy and Environment*, **25**, pp. 441-475, 2000.
25. Stocker et al., IPCC Third Assessment Report, Chapter 7: Physical Climate Processes and Feedbacks. Climate Change 2001: The Scientific Basis, Cambridge Univ. Press, 2001.

26. J. J. Bates, R. Fu, B.J. Soden, and A. Chedin, Upper tropospheric water vapor: Its radiative properties and applications in weather and climate, submitted *Rev. of Geophys.*, 2001.
27. E. K. Schneider, B. P. Kirtman, and R. S. Lindzen, Tropospheric water vapor and climate sensitivity, *J. Atmos. Sci.*, **56**, pp. 1649-1658, 1999.
28. D.-Z. Sun, and R. S. Lindzen, Distribution of tropical tropospheric water vapor, *J. Atmos. Sci.*, **50**, pp. 1643-1660, 1993.
29. S. Schroeder, and J. P. McGuirk, Widespread tropical atmospheric drying from 1979 to 1995, *Geophys. Res. Lett.*, **25**, pp. 1301-1304, 1998.
30. D. Q. Wark, D. T. Hilleary, S. P. Anderson, and J. C. Fisher, Nimbus satellite infrared spectrometer experiment, *IEEE Trans. Geosci. Elect.*, GE-8, **4**, pp. 264-270, 1970
31. C. J. Mertens, M. G. Mlynczak, D. P. Kratz, and D. G. Johnson, Feasibility of retrieving upper tropospheric water vapor from observations of far-infrared radiation, in *Optical Spectroscopic Techniques, Remote Sensing, and Instrumentation for Atmospheric and Space Research IV*, Allen M. Larar and Martin G. Mlynczak, Editors, Proceedings of SPIE, Vol. 4485, 191-201, 2002.
32. V. Kempe, D. Oertel, R. Schuster, H. Becker-Ross, and H. Jahn, Absolute IR-spectra from the measurement of Fourier-spectrometers aboard the Meteor 25 and 28, *Acta Astronautica*, **7**, pp. 1403-1416, 1980.
33. R. A. Hanel, B. Schlachman, D. Rogers, and D. Vanous, Nimbus 4 Michelson interferometer, *Appl Opt.*, **10**, pp. 1376-1382, 1971.
34. R. A. Hanel, B. Schlachman, F. D. Clark, C. H. Prokesh, J. B. Taylor, W. M. Wilson, and L. Chaney, The Nimbus III Michelson interferometer, *Appl. Opt.*, **9**, pp. 1767-1774, 1970.
35. D. P. Butler, Z. Celik-Butler, A. Jahanzeb, and J. E. Gray, *J. Appl. Phys.*, **84**, pp. 1680, 1998.
36. D. P. Butler, Z. Çelik-Butler, R. Adam, and R. Sobolewski, *J. Appl. Phys.*, **85**, pp. 1075, 1999.
37. J. E. Gray, Z. Celik-Butler, D. B. Butler, and A. Jahanzeb, *Ferroelectrics*, **209**, pp. 517, 1998.
38. D. P. Butler, M. Almasri, and Z. Celik-Butler, 14<sup>th</sup> SPIE Annual International Symposium on Aerospace/Defense Sensing, Simulation, and Controls (AEROSENSE): Infrared Detectors and Focal Plane arrays VI, Ed: E. L. Dereniak, Orlando, FL, 24-28 April, 2000.
39. L. Palchetti, R. Rizzi, B. Carli, R. Bonsignori, B. Carli, J. E. Harries, J. Leotin, S. C. Peskett, C. Serio, and A. Suter, Reasibility study of the spaceborne radiation explorer in the far infrared (REFIR), in *Optical Spectroscopic Techniques, Remote Sensing, and Instrumentation for Atmospheric and Space Research IV*, Allen M. Larar and Martin G. Mlynczak, Editors, Proceedings of SPIE, Vol. 4485, 202-209, 2002.
40. B. R. Barkstrom, The Earth Radiation Budget Experiment (ERBE), *Bull. Amer. Meteor. Soc.*, **65**, pp. 1170-1185, 1984.
41. D. G. Johnson, Design of a far-infrared spectrometer for atmospheric thermal emission measurements, in *Optical Spectroscopic Techniques, Remote Sensing, and Instrumentation for Atmospheric and Space Research IV*, Allen M. Larar and Martin G. Mlynczak, Editors, Proceedings of SPIE, Vol. 4485, 220-224, 2002.
42. Harper, D. A., R. H. Hildebrand, R. Stiening, and R. Winston, Heat trap: An optimized far infrared field optics system, *Applied Optics*, **15**, 53-60, 1976.
43. Jucks, K. J., D. G. Johnson, K. V. Chance, W. A. Traub, J. J. Margitan, G. B. Osterman, R. J. Salawitch, and Y. Sasano, Observations of OH, HO<sub>2</sub>, H<sub>2</sub>O, and O<sub>3</sub> in the upper stratosphere; Implications for HO<sub>x</sub> photochemistry, *Geophys. Res. Let.* **25**, 3935-3938, 1998.
44. Johnson, D. G., K. W. Jucks, W. A. Traub, and K. V. Chance, Isotopic composition of stratospheric water vapor: Measurements and photochemistry, *J. Geophys. Res.*, **106**, 12,211-12,218, 2001.
45. Dobrowolski, J.A. and W.A. Traub, New Designs for Far-Infrared Beamsplitters, *Applied Optics*, **35**, 2934, 1996.
46. Leonov, V. N., and I. A. Khrebtov, HTD-Vol. 277, Thermal Phenomena at Molecular and Microscales and in Crygenic Infrared Detectors, ASME 1994, p. 77.
47. Çelik-Butler, Z., D. P. Butler, M. Almasri, A. Yardanakul, A. Yildiz, 15<sup>th</sup> SPIE Annual International Symposium on Aerospace/Defense Sensing, Simulation, and Controls (AEROSENSE): Infrared Technology and Applications XXVII, Ed: Gabor Fulop, Orlando, FL, April 16 - 20, 2001.
48. Smith, S. M., Specular reflectance of optical-black coatings in the far infrared, *Applied Optics*, **23**, 2311-2326, 1984.